Proceedings of NAMRI/SME, Vol. 40, 2012

Finite Element Modeling of Microstructural Changes in Turning of *AA7075-T651* Alloy and Validation

G. Rotella, L. Settineri
Department of Production Systems and Business Economics
Politecnico di Torino
Torino, Italy

D. Umbrello
Department of Mechanical Engineering
University of Calabria
Rende, CS, Italy

O.W. Dillon Jr, I.S. Jawahir
Institute for Sustainable Manufacturing
University of Kentucky
Lexington, KY, USA

ABSTRACT
The surface characteristics of a machined product strongly influence its functional performance. During machining, the grain size of the surface is frequently modified, thus the properties of the machined surface are different to that of the original bulk material. These changes must be taken into account when modeling the surface integrity effects resulting from machining. In the present work, grain size changes induced during turning of *AA 7075-T651* (160 HV) alloy are modeled using the Finite Element (FE) method and a user subroutine is implemented in the FE code to describe the microstructural change and to simulate the dynamic recrystallization, with the consequent formation of new grains. In particular, a procedure utilizing the Zener-Hollomon and Hall-Petch equations is implemented in the user subroutine to predict the evolution of the material grain size and the surface hardness when varying the cutting speeds (180 - 720 m/min) and tool nose radii (0.4 - 1.2 mm). All simulations were performed for dry cutting conditions using uncoated carbide tools. The effectiveness of the proposed FE model was demonstrated through its capability to predict grain size evolution and hardness modification from the bulk material to machined surface. The model is validated by comparing the predicted results with those experimentally observed.

KEYWORDS
Machining, *AA 7075-T651*, Finite Element Method (*FEM*), Dynamic Recrystallization (*DRX*).

INTRODUCTION

Nowadays, the market can be considered as a scenario where the cost reduction and product quality factors have become increasingly important when attempting to be competitive. In this context, surface integrity plays a key role because it dictates the functional performance and service-life of engineered components.

Surface characteristics of machined products such as microstructure, roughness and residual stresses are some of the important constituents determining the reliability and functional performance of a product. The aircraft industry is one of the most relevant examples where all final products must be of uniformly high quality in order to ensure high safety standards for performance over the lifetime.

Actually, expensive post-operations are used in order to correct and improve the final characteristics of the machined surface. Hence, knowledge about factors that cause microstructural improvements will contribute to a better fundamental understanding of the manufacturing process mechanics and improved knowledge-driven manufacturing process planning, as well as better prediction of the component's lifetime [1].

Therefore, accurate models, capable of predicting the surface characteristics for machined components, are needed in order to obtain feedback information on how to

improve the process thereby meeting the desired surface and sub-surface property specifications. Consequently, it is useful to have a predictive model for the microstructural changes as a function of the machining conditions [2,3].

Microstructural changes in turning can be defined as a combination of "dynamic events", produced by plastic deformation and "static events", due to residual stress and residual strain. Among the dynamic events, work hardening and dynamic recovery occur during the deformation process on the workpiece. If the total local dislocation density exceeds a critical value, dynamic recrystallization (*DRX*) occurs in the corresponding region of the deforming workpiece and the microstructure drastically changes. When it occurs, this is one of the most important microstructure evolution processes because it is near the product surface, affecting the functional performance.

The material considered in this work is the 7075 series of aluminum containing zinc, magnesium, and copper as alloying elements, and this provides the highest strength of any commercial series of aluminum alloys. This material is mainly employed for aerospace, automotive and defense applications.

For this material, several mechanisms of dynamic recrystallization have been reported depending on the imposed deformation conditions as well as the chemical composition of the alloy [4-8].

Dynamic recrystallization in metals can occur mainly in two forms: continuous dynamic recrystallization (*CDRX*) and discontinuous dynamic recrystallization (*DDRX*). The dynamically recrystallized grains, during *DDRX* are formed by nucleation and grain growth and they are usually coarse and heterogeneously distributed throughout the deformation matrix.

The mechanism of *CDRX* mainly originates small, and is with uniformly distributed grains within the original grain boundaries. It is predominantly activated by progressive accumulation of dislocations in low angle boundaries, an increase of their misorientation leading to the formation of high angle boundaries within the grains. For aluminum and its alloys contrasting mechanism for dynamic recrystallization and recovery have been proposed.

The main theory related to microstructural alteration of aluminum alloy is the *CDRX* which occurs in high stacking fault energy metals where new grains are formed [7,9].

Basically, aluminum alloys, as well as beta titanium or ferritic steels, are considered metals having high efficiency of dynamic recovery, thus new grains are not formed by the classical nucleation mechanism, but the microstructure develops by progressive transformation of subgrains into new grains within the deformed original grains. Other researchers also address a more complex form of *DRX* in aluminum, as geometric dynamic recrystallization (*GDRX*) or multiple simultaneous phenomena depending on the value of the Zener-Hollomon parameter [6,10].

The objective of the proposed work is to model the effects of cutting speed and tool geometry on the grain size evolution induced by the deformation conditions that exist during the turning of *AA 7075-T651* alloy bars.

In particular, a detailed approach is presented in order to develop a FE model suitable for predicting different microstructural changes during the turning operation.

In this analysis, an iterative procedure was utilized for calibrating the constants present in the Zener-Hollomon parameter - associated with grain refinement and the Hall-Petch equation - for the hardness evolution in the selected material. Empirical models are in fact very useful in practical situations instead of physically-based models since they could be easily implemented in FE codes and, through their calibration the grain refinement and the hardness modification can be properly simulated [11].

Finally, to validate the proposed FE strategy, the numerical results were compared with those resulting from experiments.

EXPERIMENTAL PROCEDURE

The accuracy of the results obtained by using finite element methods strongly depends on the accuracy of the input values for the calibration. Thus, in order to obtain a correct prediction of the dynamic recrystallization phenomenon, an experimental program was developed and carried out. The experimental turning tests were performed under dry condition with no coolant.

Table 1. Mechanical properties of the as received material.

Mechanical properties of *AA 7075-T651*	
Ultimate Tensile Stress	612.9 MPa
Yield Tensile Stress	552.9 MPa
Elongation %	11
Hardness	160 HV
Average grain size	30 μm

The workpiece material is the *AA 7075-T651* alloy and it is a very attractive material to be utilized in the automotive and aerospace industries. The main reason for this is the good combination of properties such as fracture toughness, high strength to density ratio and resistance to stress corrosion cracking [12,13].

The initial bars were obtained by extrusion, the mechanical properties and the standard chemical composition of the material are given in Tables 1 and 2.

Table 2. Chemical composition of the as received material.

Chemical composition of *AA 7075-T651* WT%							
Si	*Fe*	*Cu*	*Mn*	*Mg*	*Cr*	*Zn*	*Ti*
0.08	0.17	1.40	0.03	2.70	0.19	6.10	0.20

The T651 treatment process includes artificially aging of the material and then stress relieving it. More precisely,

it involves a 1.5% stretch prior to 24 hours at 121°C, followed by air cooling.

The turning experimental set-up is shown in Figure 1. The machining tests were conducted on a stiff high speed Mazak *QuickTurn 10* CNC lathe in an external turning operation using uncoated carbide tools (KENNAMETAL grade: K313 with a clearance angle of 11° inserts ANSI TPG-431-2-3 geometries) with a triangular shape mounted on a CTGPL164C tool holder providing a lead angle of 0°.

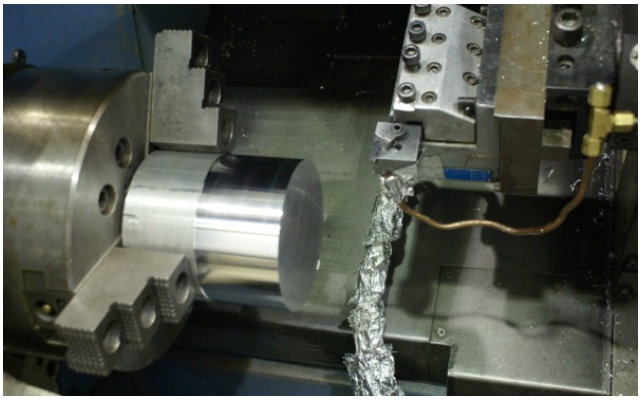

Figure 1. Experimental setup of turning tests.

Since the effective edge radius of the tool plays a very important role while turning, each cutting tool edge was measured using a Zygo®7300 optical interferometry-based surface profilometer and only the consistent tools were selected for the machining tests (Figure 2). The average tool edge radii were around 16 µm.

The tool holder was held in a Kistler 9121 three-component piezoelectric dynamometer for measuring forces.

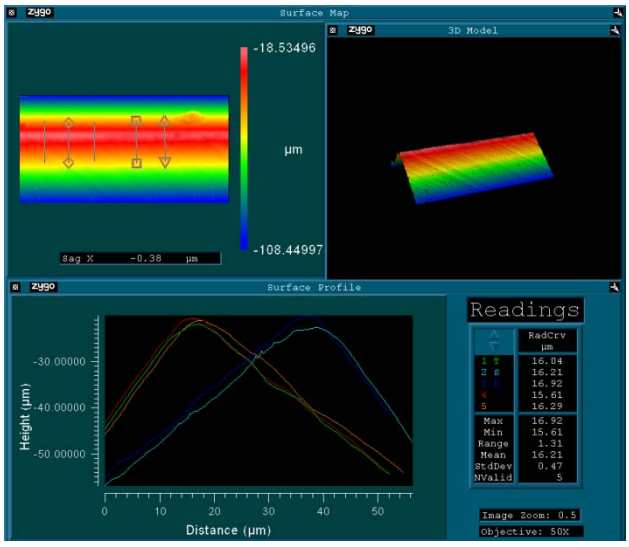

Figure 2. Measured tool edge radius by means of Zygo profilomiter.

The performed tests were carried out at a constant depth of cut of 0.5 mm and feed 0.1 mm/rev while the cutting speed and tool geometry were varied as follows:

- Test 1: V_c = 180 m/min – nose radius, R = 0.8 mm
- Test 2: V_c = 320 m/min – nose radius, R = 0.4 mm
- Test 3: V_c = 320 m/min – nose radius, R = 0.8 mm
- Test 4: V_c = 320 m/min – nose radius, R = 1.2 mm
- Test 5: V_c = 720 m/min – nose radius, R = 0.8 mm

After each test, the final surface microstructure and the hardness profile of the machined samples were measured.

The average values of the three cutting force components (directions are shown in Figure 3), calculated on the acquired signals when mechanical steady-state condition was reached, are reported in Figures 4-6.

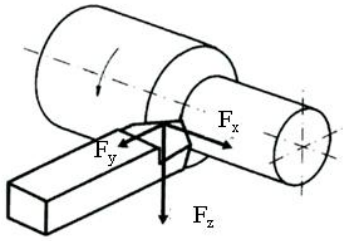

Figure 3. Directions of the cutting forces acting during the machining process.

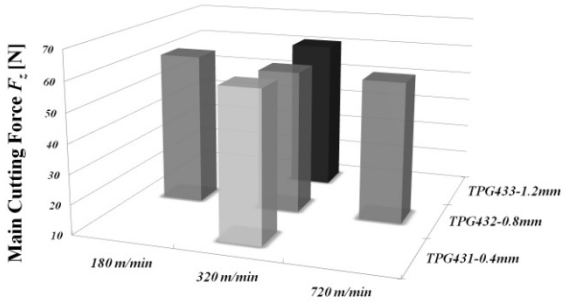

	180 m/min	320 m/min	720 m/min
TPG431-0.4mm		60.05	
TPG432-0.8mm	61.05	58.05	57.30
TPG433-1.2mm		60.75	

Figure 4. Influence of the cutting speed and tool nose radius on the measured main cutting force, F_z (Depth of cut = 0.5 mm and Feed rate = 0.1 mm/rev).

As expected, the forces components are influenced by the tool geometry and the cutting speed. More specifically, very small changes are detected for the main cutting force at varying of cutting speed and tool nose radii (Figure 4). The feed force, F_x, decreases when the cutting speed is increased; furthermore, it is strongly influenced by the tool nose radius: lower values of the radius generate the highest feed force (Figure 5). Similarly, the radial force is influenced by the tool geometry since it increases by increasing the nose radius, while it slightly decreases with the increase of the cutting speed (Figure 6).

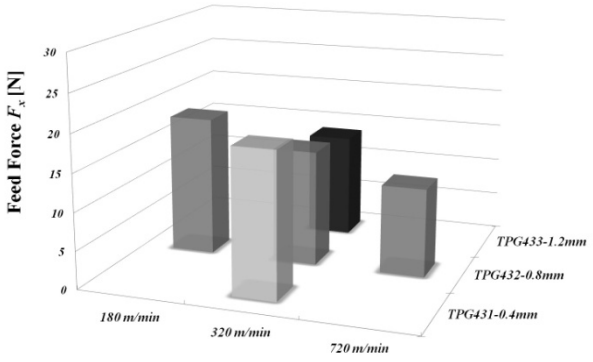

	180 m/min	320 m/min	720 m/min
TPG431-0.4mm		19.12	
TPG432-0.8mm	18.42	15.24	11.71
TPG433-1.2mm		13.71	

Figure 5. Influence of the cutting speed and tool nose radius on the measured feed force, F_x (Depth of cut = 0.5 mm and Feed rate = 0.1 mm/rev).

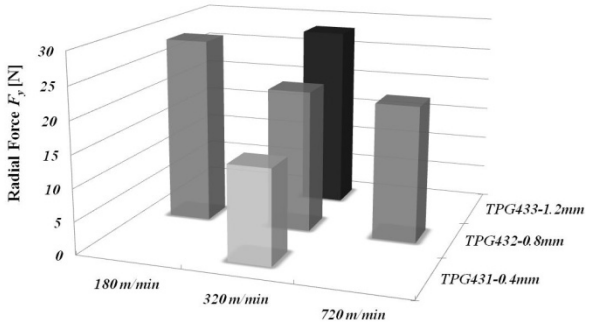

	180 m/min	320 m/min	720 m/min
TPG431-0.4mm		14.47	
TPG432-0.8mm	28.50	21.80	20.90
TPG433-1.2mm		28.13	

Figure 6. Influence of the cutting speed and tool nose radius on the measured radial force, F_y (Depth of cut = 0.5 mm and Feed rate = 0.1 mm/rev).

The micro hardness, Vickers $HV_{0.05}$, of each sample was also measured in order to verify the microstructural changes in the machined samples. The results shown in Figures 7 and 8 demonstrate that the hardness increases on the surface and in the subsurface (within the affected layer) from that measured in the bulk material varying with both the cutting speed and tool nose radius.

In particular, the cutting speed seems to have a smaller influence on the final surface hardness (Figure 7). On the contrary, it significantly affects the subsurface since a higher cutting speed produces higher hardness values at a given depth in the subsurface and causes deeper microstructural alteration.

The nose radius also has an influence on the hardness modification of the *AA 7075* finished product both on the surface and subsurface. In fact, a higher tool nose radius produces higher hardness values and deeper microstructural modification.

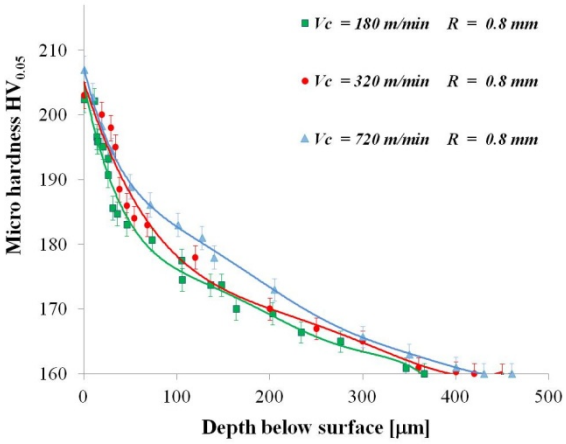

Figure 7. Measured hardness near the machined samples at varying cutting speeds.

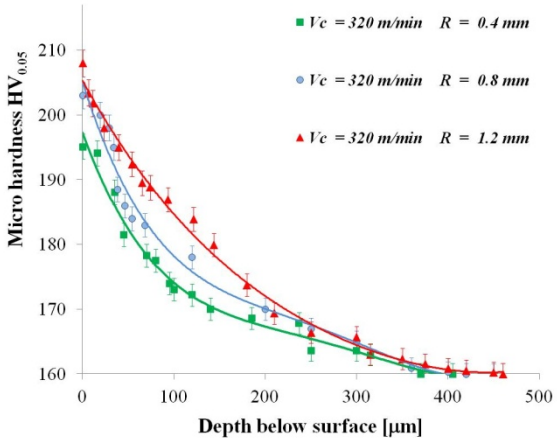

Figure 8. Measured hardness on the machined samples when using varying tool nose radii.

The grain size of each machined surface has also been measured, and it was found that the recrystallization occurs in all investigated cases. More precisely, all the examined samples presented a refinement of the mean grain diameter from the bulk to the surface as represented in Figure 9 where the optical images for Test 5 are reported.

The values for the measured grain size in each test are reported in Table 3, highlighting how the cutting parameters and the geometry of the tool can influence the final microstructure of the machined product. In fact, grain size becomes smaller when higher cutting speed and tool nose radii are utilized, although the cutting speed seems to have a higher influence on the microstructural changes than the tool nose radius reflecting a higher value of the Zener-Hollomon parameter.

Table 3. Measured average grain size on machined surface varying the cutting process parameters.

Test	V_c [m/min]	R [mm]	Average grain size on machined surface [μm]
1	180	0.8	12.39
2	320	0.4	12.33
3	320	0.8	10.10
4	320	1.2	7.73
5	720	0.8	4.05

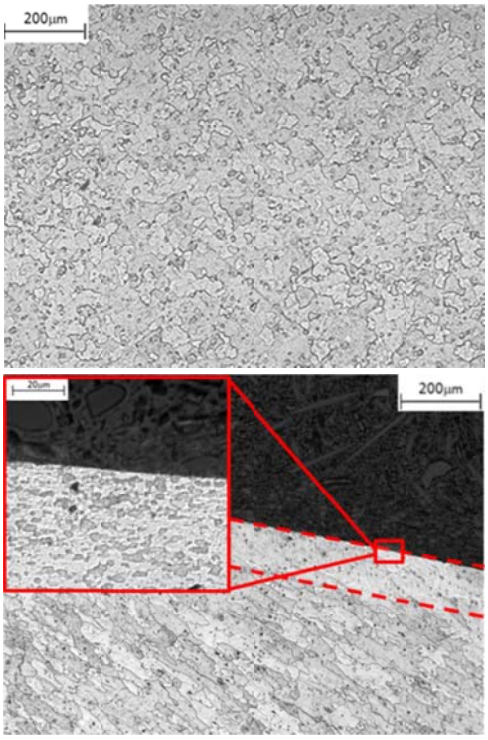

Figure 9. Optical images of the bulk material (a) and the machined surface (b): Test 5.

FE NUMERICAL PROCEDURE

Numerical simulations is a very attractive technique capable of predicting, if properly calibrated, the thermal and mechanical behavior of a processed material. This saves time and money that would be necessary to perform the extensive experiments. Therefore, both productivity and costs can benefit from the use of numerically calibrated techniques.

The Finite Element (FE) software chosen to simulate the process is SFTC-Deform 3D™. The calibration of the proposed model was carried out by comparing the FE predicted results with those determined experimentally for Test 3. In particular, the aim of this calibration phase was to determine the frictions values (m and μ) to be set in the sticking-sliding model (sticking governed by the shear model $\tau = m\tau_0$; sliding governed by Coulomb model $\tau = \mu\sigma$) and the global heat transfer coefficient (h_{int}) to be defined at the tool-chip and tool-workpiece interfaces. At the end of the iterative procedure, the chosen values were: $m = 0.9$ and $\mu = 0.4$ which represent the best trade-off for the sticking-sliding model. Using the proposed iterative procedure, the global heat transfer coefficient, h_{int}, at the tool-chip and tool-workpiece was also found, being equal to 55000 kW/m^2K. This value permits one to reach the thermal steady-state at the tool-chip-workpiece interfaces within a short simulation time by means of the assumption of thermally perfect contact under high cutting pressures.

Once the mechanical and thermal calibrations were carried out, a user subroutine was implemented to predict the dynamic recrystallization process and the hardness modification (Figure 10).

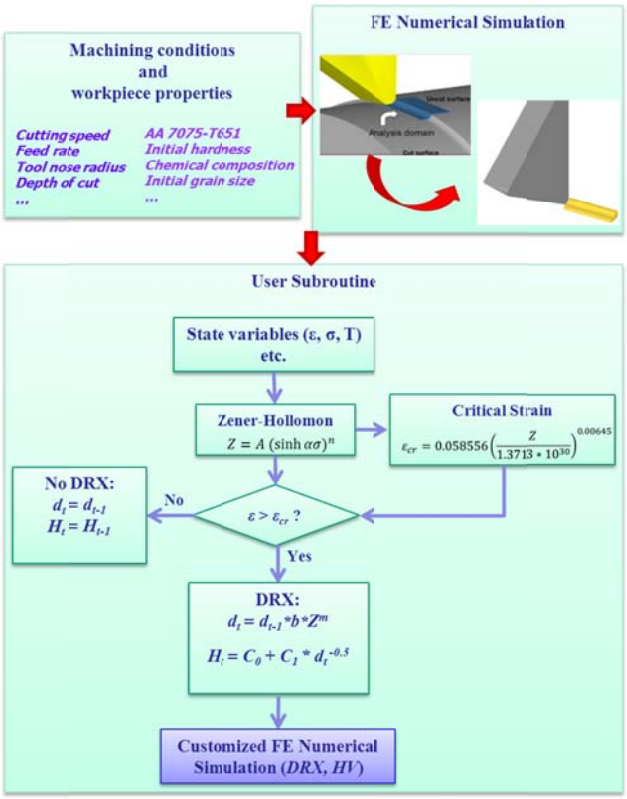

Figure 10. Structure of the user routine for predicting the grain size and hardness.

In the user routine, Zener-Hollomon equation has been used to predict the dynamic recrystallization, while the hardness variation has been taken into account using the Hall-Petch equation. More in detail, the Zener-Hollomon parameter is defined as following [14]:

$$Z = \dot{\varepsilon}\, exp\left(\frac{Q}{RT}\right) \quad (1)$$

where is the strain-rate, R = 8.3145 J/(K*mol), is the universal gas constant; Q = 116.7 kJ/mol, is the apparent activation energy for mechanical deformation process; T is the absolute temperature, K. Alternatively, the constitutive Zener-Hollomon equation is defined as [15]:

$$Z = A\,(\sinh \alpha\sigma)^n \tag{2}$$

where α and n are two constants in the constitutive equation and found to be 0.012 mm^2/N and 5.3, respectively [15].

The recrystallized grain size is related to the Zener-Hollomon parameter as [14]:

$$d = d_0 * b * Z^m \tag{3}$$

where d_o is the initial grain size in μm, b and m are two material constants.

As far as the hardness is regarded, it is related to the recrystallized grain size as [16]:

$$HV = C_0 + C_1 * d^{-0.5} \tag{4}$$

The guard parameter able to activate the dynamic recrystallization is the critical strain, ε_{cr}. This value was calculated by the equation proposed by Quan et al [17] shown in Figure 10 and it was found to have a mean value of 0.06 in accordance with values found in Rokini et al [8] for the same Aluminum alloy. In a generic time step (t), ε_{cr} is evaluated and it is compared with the actual strain given by FE simulation; if the latter is higher than the critical value, the recrystallization takes place and a new grain size is calculated using the Zener-Hollomon parameter (Equation 3) as well as the new hardness value is calculated according to the Hall-Petch equation (Equation 4). The values are updated in the next time step of the FE code.

On the contrary, if the recrystallization could not take place due to the low value of strain, the Equations 3 and 4 are not applied, and both the grain size and the hardness remain unchanged from the previous step (t-1) as shown in Figure 10.

It is important to underline that the model for the dynamic recrystallization implemented in the user routine (Equation 3) is based on the assumption that after the dynamic recrystallization phase there is no grain growth taking place on the machined sample.

In order to verify the reliability of this assumption, the average grain size on the machined surface was measured at different cutting time (i.e., different lengths on the machined bar) for Test 1 (Figure 11).

The selection of a different test, other than the calibration one, was made in order to increase the duration of the test and to evaluate the possible grain growth in the worst case corresponding with the longest experiment in time. The observed results, as reported in Figure 11, demonstrate that no significant grain size differences at different cutting times are observed, confirming that the recrystallized grains did not grow after the microstructural changes directly induced by machining.

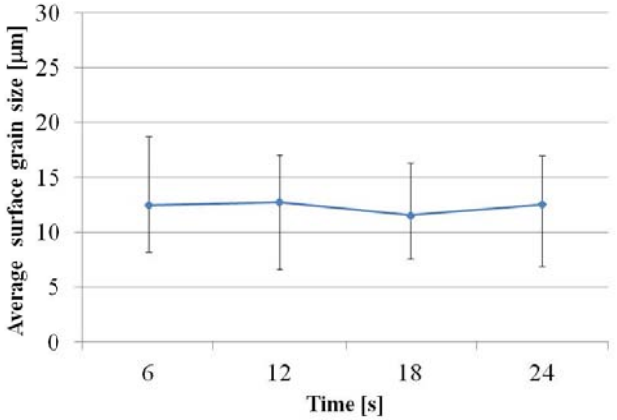

Figure 11. Average grain size evolution on machined surface vs. cutting time for Test 1.

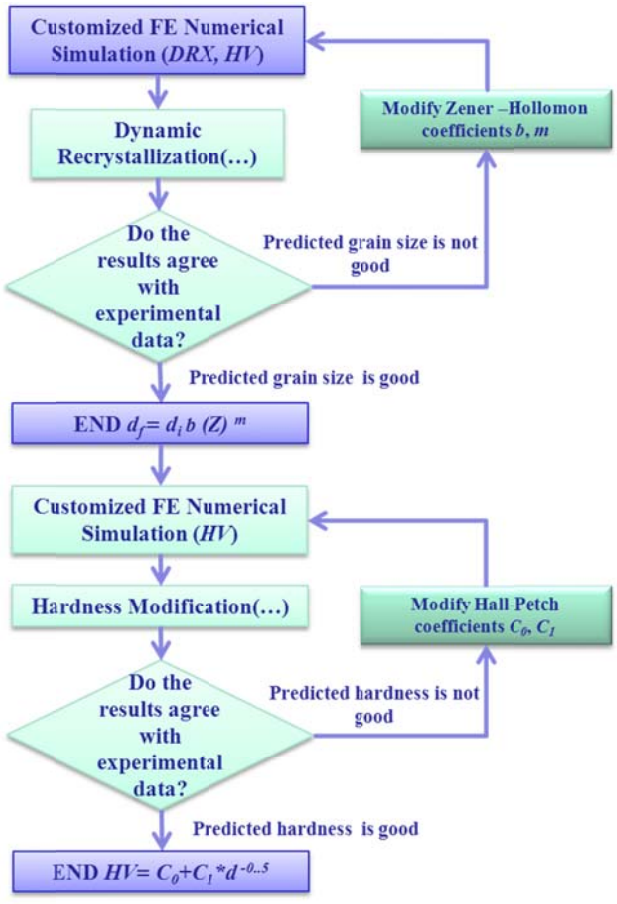

Figure 12. Calibration procedure of the implemented user routine for predicting the grain size and hardness.

The described user routine requires to be calibrated in order to define the two constants in the Zener-Hollomon parameters as well as those in the Hall-Petch equation; therefore an analysis was carried out to understand the influence of the single parameters on the grain size and hardness values, subsequently a "trial and error" procedure (Figure 12) has been performed in order to obtain the correct values for all the needed constants.

The calibration phase started based on the data reported by Cerri et al [18] thus, their Zener-Hollomon constants were used as the starting point for the constants calibration phase. Due to the nature of the exponential equation, the constant b has a lower influence on the grain size modification rate while the parameter m had a greater influence. Also for the Hall-Petch equation two initial values of constants C_0 and C_1 were set, derived from the initial specimen conditions (i.e., initial grain size and hardness).

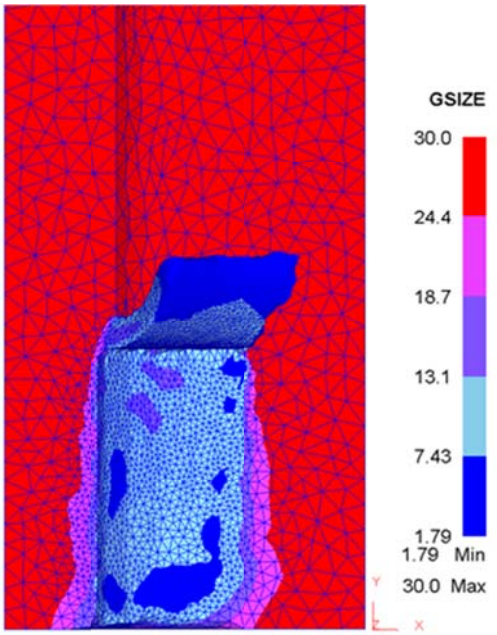

Figure 13. Predicted grain size [μm] after calibration of Zener-Hollomon coefficients.

The cutting conditions for the calibration phase were set equal to the experimental condition of Test 3 (the same used for mechanical and thermal calibration): cutting speed of 320 m/min, feed rate of 0.1 mm/rev, tool nose radius of 0.8mm. The cutting tool material used is K313 grade uncoated carbide tool and the relative mechanical, thermal and physical properties were set in the FE model.

Figures 13 and 14 report the calibration results for the code for the grain size and the hardness; in particular the numerical value of grain size obtained near the machined surface varied from 7.43 to 13.11 μm with a mean value of 9.71 μm, and this is in agreement with the value of about 10 μm found experimentally.

The surface hardness value found at the end of the calibration phase was also in agreement with those experimentally measured since the numerical value on surface ranged from 192 to 223 HV with an average value of 200.5 HV, very close to the average experimental value of 203 HV.

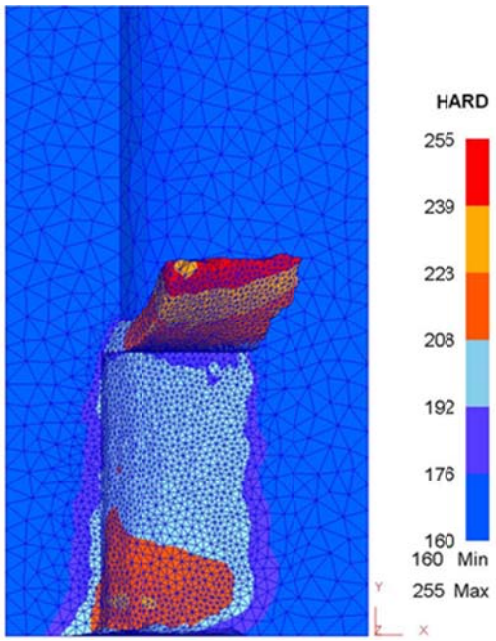

Figure 14. Predicted Vickers hardness variation after calibration of the Zener-Hollomon coefficients.

Furthermore, the thickness of the affected layer in the calibration phase (Figure 15) was also taken into account in order to verify the reliability of the critical strain equation, ε_{cr} (Figure 10). Particularly, it was found that the numerically estimated thickness of the affected layer was similar to those experimentally observed in Figures 7 and 8 and in which the hardness modification is relieved.

Finally, the coefficients b and m calculated at the end of the calibration were respectively equal to 54300 and -0.25.

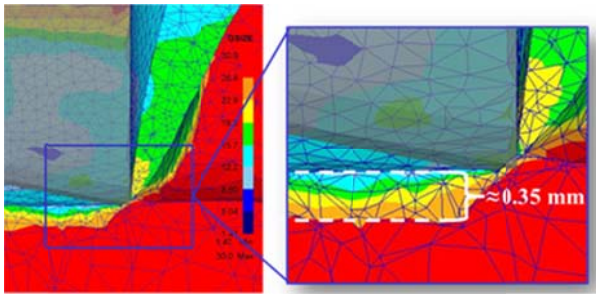

Figure 15. Predicted affected layer obtained by FE analysis on the calibration Test 3.

Validation phase

After the calibration phase, the FEM model has been validated by comparing the experimental data with other corresponding simulation results. The user routine (Figure 10) was used to predict the evolution in material grain size and hardness at different cutting speeds of 180 m/min, 320 m/min and 720 m/min and three different tool nose radii of 0.4 mm, 0.8 mm and 1.2 mm.

Figures 16-18 show the comparison between the measured and the predicted forces. The predicted force trend is always aligned with the one found in the experiments, although in some cases a discrepancy can be noted, especially for the radial force.

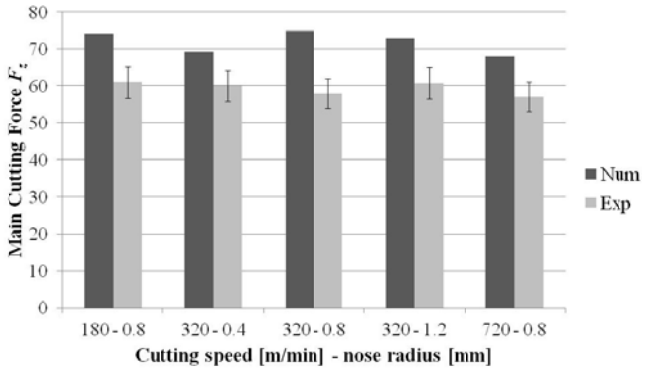

Figure 16. The comparison of the measured and the predicted main cutting force, F_z, during machining.

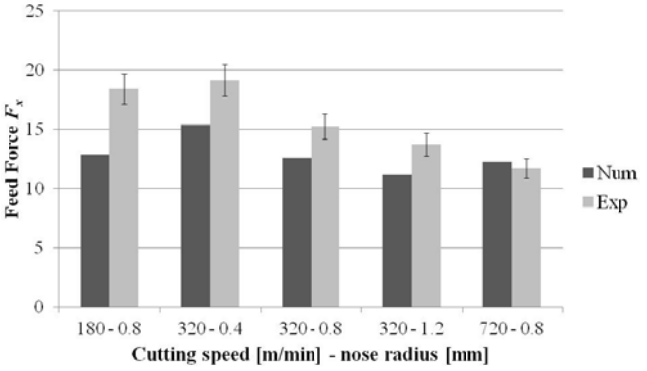

Figure 17. The comparison of the measured and the predicted feed force, F_x, during machining.

These numerical difficulties for predicting the cutting forces in 3D FE analysis, are still a problem under investigation within the scientific community. The problem might be related to the friction models used which are well tested in orthogonal machining, but they are not yet for 3D machining in which other important tool geometry parameters are involved (tool nose radius, angles, etc.) as well as the influence of grain size on the friction coefficient.

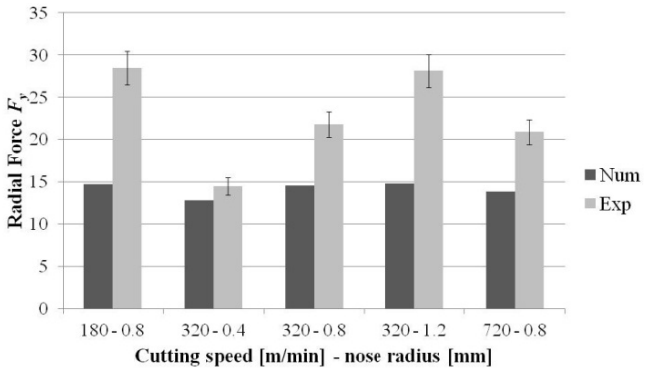

Figure 18. The comparison of the measured and the predicted radial force, F_y, during machining.

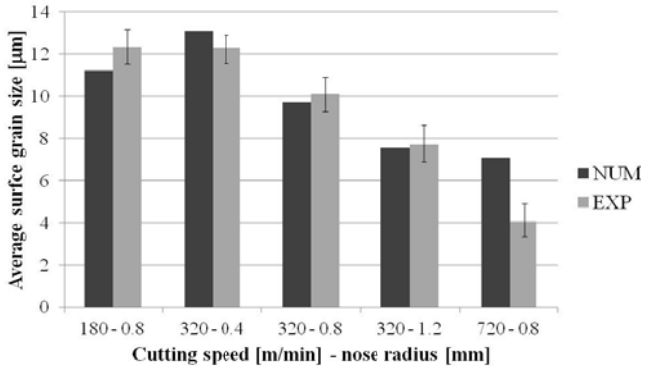

Figure 19. The comparison of the measured and the predicted surface grain size.

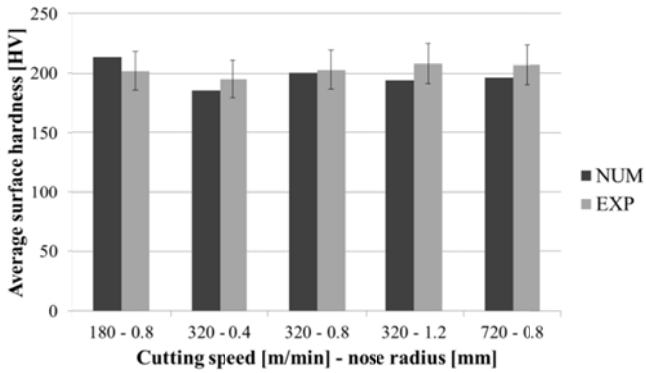

Figure 20. The comparison of the measured and the predicted surface hardness.

In contrast, a good agreement was found in the prediction of both grain size (Figure 19), and the surface hardness on the machined workpiece (Figure 20) for each validation test. This highlights the result that, once calibrated, the utilized FE model and the implemented user routines well predict the parameters that relate to the surface integrity and surface characteristics.

CONCLUSIONS

In this paper a FE model is proposed for studying the turning process of *AA7075-T651* alloy in terms of grain size and hardness prediction. The Zener-Hollomon parameter was employed for relating the deformation conditions to the recrystallized grain size while the Hall-Petch equation was employed for the hardness; the simulation results were validated with experimental data from performed tests.

The numerical results show a good prediction of the microstructural alteration occurring during machining of the workpiece (under certain conditions).

Particularly it was found that both the cutting speed and the tool nose radius affect the machined surface and subsurface integrity since both dynamic recrystallization and higher hardness values were observed.

In the near future, the FE model will be further developed to simulate the influence of liquid nitrogen-based cryogenic cooling by adjusting the thermal boundary conditions based on experimentally measured data during cryogenic machining. Finally, the proposed FE model to predict the dynamic recrystallization and the grain size distribution on the machined surface will be used to better understand and control the final performance of the product such as its fatigue life under service [19].

AKNOLEDGEMENTS

The authors gratefully thank the Institute for Sustainable Manufacturing (University of Kentucky) for their support and Mr. Charles Arvin and Mr Tao Lu for their help with the machining experiments. The authors also would like to acknowledge Kennametal Inc. (Mr. Steve Chen) for their support with free cutting tools and tool holders and Dr. Aldo Attanasio (University of Brescia) for his help with the FE analysis.

REFERENCES

[1] Jawahir, I.S., Brinksmeier, E., M'Saoubi, R., Aspinwall, D.K., Outeiro, J.C., Meyer, D., Umbrello, D., Jayal, A.D., 2011, Surface integrity in material removal processes: Recent advances, CIRP Annals - Manufacturing Technology 60(2), 603–626.

[2] Campbell, C.E., Bendersky, L.A., Boettinger, W.J., Ivester, R., 2006, Microstructural characterization of Al-7075-T651 chips and work pieces produced by high-speed machining, Materials Science and Engineering A 430, 15-26.

[3] Davim, J.P., Maranhão, C., Jackson, M.J., 2008, FEM analysis in high speed machining of aluminium alloy (Al7075-0) using polycrystalline diamond (PCD) and cemented carbide (K10) cutting tools, Int J Adv Manuf Technol 39, 1093-1100.

[4] Gottstein, G., Kocks, U.F., 1983, Dynamic Recrystallization and Dynamic Recovery in <111> single crystals of Nickel and Copper, Acta Metall. 31, 175-188.

[5] McQueen, H.J., 2004, Development of dynamic recrystallization theory, Materials Science and Engineering A 387-389, 203-208.

[6] Kassner, M.E., Barrabes, S.R., 2005, New developments in geometric dynamic recrystallization, Materials Science and Engineering A 410-411, 152-155.

[7] Gourdet, S., Montheillet. F., 2003, A model of continuous dynamic recrystallization, Acta Materialia 51, 2685–2699.

[8] Rokini, M.R., Zarei-Hanzaki, A., Roostaei, A.A., Abedi, H.R., 2011, An investigation into the hot deformation characteristics of 7075 aluminum alloy, Materials and Design 32, 2339–2344.

[9] Sakai, T., Miura, H., Goloborodko, A., Sitdikov, O., 2009, Continuous dynamic recrystallization during the transient severe deformation of aluminum alloy 7475, Acta Materialia 57, 153-162.

[10] Liu, C., Jiang, S., Zhang, X., .2005, Continuous dynamic recrystallization and discontinuous dynamic recrystallization in 99.99% polycrystalline aluminum during hot compression, Trans. Nonferrous Met. Soc. China 15, 82-86.

[11] Bariani, P.F., Dal Negro, T., Bruschi, S., 2004, Testing and Modelling of Material Response to Deformation in Bulk Metal Forming, Annals of CIRP 53/2, 573-596.

[12] Heinz, A., Haszler, A., Keidel, C., Moldenhauer, S., Benedictus, R., Miller, W.S., 2000, Recent development in aluminum alloys for aerospace applications, Materials Science and Engineering A 280, 102-107.

[13] Immarigeon, J.P., Holt, R.T., Koul, A.K., Zhao, L., Wallace, W., Beddoes, J.C., 1995, Lightweight materials for aircraft applications, Materials Characterization 35, 41-67

[14] Yanagimoto, J., Karhausen, K., 1998, Incremental Formulation for the Prediction of Flow Stress and Microstructural Change in Hot Forming, Journal of manufacturing science and engineering 120(2), 316-322.

[15] Sheppard, T., Tunnicliffe, P.J., Patterson, S.J., 1982, Direct and Indirect Extrusion of a High Strength Aerospace Alloy (AA7075), Journal of Mechanical Working Technology 6, 313-331.

[16] Hughes, G.D., Smith, S.D., Pande, C.S., Johnson H.R., Armstrong, R.W., 1986, Hall-Petch strenghening for the microhardness of twelve nanometer grain diameter electrodeposited Nickel, Scripta Metallurgica 20, 93-97.

[17] Quan, G.Z., Mao, Y.P., Li, G.S., Lv, W.Q., Wang, Y., Zhou, J., 2012, A characterization for the dynamic recrystallization kinetics of as-extruded 7075 aluminum alloy based on true stress–strain curves, Computational Material Science 55, 65-72.

[18] Cerri, E., Evangelista, E., Forcellese, A., McQueen, H.J., 1995, Comparative hot workability of 7012 and 7075 alloys after different pretreatments, Materials Science and Engineering A 197, 181-198.

[19] Rotella, G., Lu, T., Settineri, L., Dillon, O.W., Jawahir, I.S., 2011, Dry and Cryogenic Machining: Comparison from the Sustainability Perspective, Proceedings of 9th Global Conference on Sustainable Manufacturing, 99-104